

Recoil alignment in muon capture on nitrogen-14

T.P. Gorringer,¹ D.P. Corbin,¹ T.J. Stocki,²

¹ *University of Kentucky, Lexington, KY 40506*

² *University of British Columbia, Vancouver, B.C., Canada V6T 1Z1*

(November 5, 2018)

Abstract

We report a measurement of the longitudinal alignment A_L of the recoil nucleus in the $\mu^- + {}^{14}\text{N}(1^+, 0) \rightarrow \nu_\mu + {}^{14}\text{C}(2^+, 7012)$ transition. The experiment was performed on the M9B beamline at the TRIUMF cyclotron via the measurement of the Doppler lineshape of the subsequent ${}^{14}\text{C}(2^+, 7012) \rightarrow {}^{14}\text{C}(0^+, 0)$ gamma-rays. We compare our result $A_L = 0.60 \pm 0.11$ to various model calculations, and discuss the sensitivity to the induced pseudoscalar coupling, second-forbidden effects and $2\hbar\omega$ wavefunction admixtures.

23.40.-s, 23.40.Hc, 27.30.+t

arXiv:nucl-ex/0410011v1 8 Oct 2004

I. INTRODUCTION

Muon capture by complex nuclei has been used in the study of both the dynamics of the weak interaction and the structure of the atomic nucleus. Generally, in exclusive capture between discrete states one attempts to separate the effects of dynamics and structure by suitable choice of physical observables and spin-parity sequences. Of course in practice these dual aspects of muon capture are not completely separable, and inevitably such studies must confront the entanglement of dynamics and structure.

Of special interest in muon capture is the induced pseudoscalar coupling constant g_p of the nucleon's weak axial current A_μ . Its value is firmly predicted by chiral symmetry [1–3] thus making its measurement an important test of low energy QCD. Moreover, in complex nuclei its medium modification – due to effects that range from core polarization and exchange currents to partial restoration of chiral symmetry [5–7] – are of considerable interest. Unfortunately, the world data on g_p from exclusive capture on complex nuclei is rather sparse, it comprising the study of recoil orientations in allowed Gamow-Teller transitions on ^{12}C [8–11] and ^{28}Si [12–14], the study of hyperfine effects in allowed Gamow-Teller transitions on ^{11}B [15,16] and ^{23}Na [17,18], and the measurement of the $^{16}\text{O}(0^+, 0) \rightarrow ^{16}\text{N}(0^-, 120)$ first-forbidden transition rate [19–21]. While the majority of these experiments are in agreement with the chiral prediction for the induced coupling, the result of $g_p/g_a = 1.0_{-1.2}^{+1.1}$ [4] from the ^{28}Si experiments is in stark disagreement with the theoretical expectation.

It is perhaps surprising – given that fifty years have passed since the birth of $V-A$ theory – that few measurements of recoil orientations in muon capture have actually been performed. Partly motivated by the puzzling result for the recoil orientation in the $^{28}\text{Si}(0^+, 0) \rightarrow ^{28}\text{Al}(1^+, 2201)$ experiment, we therefore decided a further investigation of recoil orientations in exclusive capture was worthwhile. The case we chose was $^{14}\text{N}(1^+, 0) \rightarrow ^{14}\text{C}(2^+, 7012)$, it presenting an interesting example of the different sensitivities of the different observables to the weak dynamics and the nuclear structure.

Herein we report the measurement of the recoil alignment in the transition $^{14}\text{N}(1^+, 0) \rightarrow ^{14}\text{C}(2^+, 7012)$. In Sec. II we briefly outline the measurement technique and experimental setup. The determination of the recoil alignment from the Doppler broadened spectrum of the 7012 keV gamma-rays is described in detail in Sec. III. In Sec. IV we compare our experimental result to model calculations, and discuss the sensitivity to the induced pseudoscalar coupling g_p , second-forbidden contributions, and $A = 14$ nuclear wavefunctions. Note that gamma-ray intensities from this $\mu^{-14}\text{N}$ experiment were published earlier in Stocki *et al.* [22].

II. DOPPLER METHOD AND EXPERIMENTAL SETUP

The products of exclusive muon capture are a left-handed muon neutrino and an oriented recoil nucleus. The recoil orientation is a direct manifestation of the $V-A$ character of the weak interaction, and for certain spin-parity sequences the induced coupling g_p has a large effect on the recoil orientation. Moreover, in appropriate cases the recoil orientation can be experimentally determined from the directional correlation that is imparted on either the beta-rays or the gamma-rays that are subsequently emitted by the unstable recoil.

A method for measuring the γ -recoil directional correlation was originally proposed by Grenacs *et al.* [23]. The method takes advantage of the Doppler shift of the γ -ray energy for a decay in-flight. If the recoil is in motion as it decays its energy is shifted by

$$\frac{\Delta E}{E_o} = \frac{E - E_o}{E_o} = \beta \cos \theta \quad (1)$$

where E_o is the γ -ray energy in the recoil reference frame, E is the γ -ray energy in the laboratory reference frame, $\beta = v/c$ is the velocity of the recoil in the laboratory, and θ is the angle between the γ -ray momentum vector and the recoil momentum vector. Consequently the lineshape of the Doppler broadened γ -ray is a reflection of the γ -recoil angular correlation. In suitable cases, *i.e.* where the γ -ray lifetime is short and the spin-parity sequence is sensitive, this method thus permits the determination of the recoil orientation in the capture process.

In this work we have studied the sequence $^{14}\text{N}(1^+, 0) \rightarrow ^{14}\text{C}(2^+, 7012) \rightarrow ^{14}\text{C}(0^+, 0)$. Because the lifetime of the 7012 keV state is rather short, 9.0 ± 1.4 fs [24], and the slowing-down time of the ^{14}C recoil in a liquid N_2 target is rather long, ~ 0.8 ps [25], the γ -ray spectrum is Doppler broadened. The resulting γ -recoil angular distribution is given by [26–29]

$$W(\theta) = 1 + A_L B_2 P_2(\cos \theta) \quad (2)$$

where $P_2(\cos \theta)$ is the Legendre polynomial, A_L is the recoil's longitudinal alignment and B_2 is the γ -decay correlation coefficient.¹ Note that the longitudinal alignment A_L is a direct manifestation of the different populations of the magnetic sub-states about the recoil direction, and is entirely governed by the capture process. Conversely the γ -decay coefficient B_2 is a function of the γ -decay. For a $2^+ \rightarrow 0^+$ transition and a rank-2 orientation its value is $B_2 = -\sqrt{\frac{5}{14}}$ [29]. For further details see Appendix A.

A detailed discussion of the experimental setup was presented in Stocki *et al.* [22] – herein we review the features that are important for the determination of the recoil alignment A_L in the $^{14}\text{N}(1^+, 0) \rightarrow ^{14}\text{C}(2^+, 7012)$ transition. The experiment was conducted on the M9B superconducting muon channel at the TRIUMF cyclotron. The negative muon beam had a momentum of 65 MeV/c and a flux of $2 \times 10^5 \text{s}^{-1}$, with an electron contamination of $\sim 20\%$ and a pion contamination of $< 0.2\%$. The incoming particles were detected in a three-element plastic scintillator beam telescope and stopped in a liquid nitrogen target. The target was 20×55 cm in cross section and 21 cm in thickness with walls of polystyrene. Mu-metal was used to reduce the ambient magnetic field and thereby the muon spin precession. The outgoing γ -rays were detected at right-angles to the beam axis in a high-purity Ge detector with a Compton suppressor. The Ge detector had an efficiency of 44%, an in-beam energy resolution of 2.5 keV, and an in-beam time resolution of 6 ns, for the 1.33 MeV γ -ray line of a Co-60 source. The Compton suppressor comprised a six-element annulus of NaI(Tl) crystals.

¹In Eqn. 2 we omit the negligible effects of rank-4 correlations and assume either unpolarized muonic atoms or perpendicular geometry (see Appendix A and Ref. [4] for further details).

A remark is warranted on the hyperfine effect in the $\mu^{-14}\text{N}$ atom. On formation the 1S ground state of the $\mu^{-14}\text{N}$ atom is a statistical mix of the two hyperfine states, *i.e.* one third $F_- = 1/2$ and two thirds $F_+ = 3/2$. Hyperfine transitions, from the higher-lying F_+ state to the lower-lying F_- state, would modify these proportions, and consequently the various observables in muon capture. Such transitions in μ -atoms are mediated by the M1 emission of an Auger electron from the surrounding electronic orbits [30,31]. For $\mu^{-14}\text{N}$, where the muonic atom hyperfine splitting is 7.4 eV and outer-most electron binding energy is 11.3 eV, one expects such transitions to be energetically forbidden [22]. We note the authors of Ref. [32] have suggested the possibility of a non-zero hyperfine transition rate via an unconventional transition mechanism in the $\mu^{-14}\text{N}$ atom. However, in absence of confirmation in recent studies by Stocki *et al* [22], we will hereafter assume that the capture originates from a statistical mixture of the hyperfine states, *i.e.* the measured recoil alignment is the statistical recoil alignment A_L^{stat} .

Finally we note the proximity of the interesting 7012 keV level to the ^{14}C neutron separation energy. This allays the concern over cascade feeding to the 7012 keV level from muon capture to a higher-lying level.

III. ALIGNMENT DETERMINATION

The resulting spectrum in the energy region of the 7012 keV γ -ray is shown in Fig. 1. The γ -ray events in Fig. 1 were recorded within a $\sim 5.0 \mu\text{s}$ time window of a muon arrival and in absence of any signal in the Compton suppressor.²

The first step in the analysis was the determination of the energy calibration and the instrumental resolution of the Ge detector. The energy calibration was obtained from eight well-known and clean γ -ray lines from thermal neutron capture on Al, Fe and Cl with energies that ranged from 6.2 MeV to 7.8 MeV [33]. In fitting the peaks we found a simple Gaussian lineshape with energy-independent width to be sufficient. A linear relation between channel number and γ -ray energy was also adequate for the calibration in the energy range 6.2-7.8 MeV.

Next we performed the least-squares fit to the Doppler lineshape of the 7012 keV γ -ray. The fit function involved the convolution of the theoretical lineshape (Eqn. 2) with the instrumental resolution of the Ge detector and the slowing-down effects in the target material. To compute the slowing-down time τ_{sd} of the ^{14}C recoil ion in the liquid N_2 target we used the computer program SRIM [25]. We note that the slowing-down time $\tau_{sd} \sim 0.8$ ps is much longer than the gamma-ray lifetime $\tau = 9.0 \pm 1.4$ fs, and consequently in incorporating the slowing-down effects into the Doppler lineshape we assumed a simple linear form $\beta(t) = \beta_o(1 - t/\tau_{sd})$ for the recoil velocity time dependence.

The energy spectrum in Fig. 1 also indicates the presence of a weak background line on

²Note that the first escape peak and the second escape peak of the 7012 keV gamma-ray were also identified, and therefore in principle were available for the determination of the Doppler lineshape. However, in practice such analysis was precluded by the poor statistics and the line backgrounds in the regions of these peaks.

the far lefthand side of the Doppler spectrum. We identified this peak as a 6978 keV gamma-ray originating from thermal neutron capture on chlorine-35. This identification was based on both its energy correspondence and reasonable consistency with observed intensities of other stronger $^{35}\text{Cl}(n, \gamma)$ lines. The $^{35}\text{Cl}(n, \gamma)$ background was believed to originate from polyvinyl chloride tape in the vicinity of the target. Consequently, both a Doppler peak and a Gaussian peak were needed to fit the region of the 7012 keV peak.

The fit function involved a total of eleven adjustable parameters. They comprised the amplitudes (A_D , A_G), centroids (X_G , X_D) and instrumental widths (σ) of the Doppler peak and the Gaussian peak, the initial velocity (β), slowing-down time (τ_{sd}) and longitudinal alignment (A_L^{stat}) of the ^{14}C recoil, and the amplitude and the slope of the continuum background. Fortunately, a number of parameters could be fixed in the fit, for example the instrumental widths and peak centroids from the energy calibration, the initial velocity from the reaction kinematics, and the recoil slowing-down time from the SRIM calculation. Also the amplitude of the 6978 keV $^{35}\text{Cl}(n, \gamma)$ line could be estimated from the amplitudes of the other $^{35}\text{Cl}(n, \gamma)$ lines and the available thermal neutron capture data [33,34].

Our benchmark fit, which clearly demonstrates the good agreement between the measured spectrum and the theoretical function, is shown in Fig. 1. In this fit the instrumental width (σ), initial velocity (β) and slowing-down time (τ_{sd}) were all fixed at their calculated values. The fit gave $A_L^{stat} = 0.60 \pm 0.11$ with a chi-squared $\chi_{pdf}^2 = 0.7$.

To investigate the correlations between the recoil alignment and the other parameters we performed a series of fits, the results of which are summarized in Table I. The Table shows that the “best-fit” value of the recoil alignment is only weakly dependent on the parameters related to the energy calibration and the instrumental resolution (rows 1-4 of Table I). In addition it shows that large changes in the input value of the slowing-down time, which ranged from $\tau_{sd} = 0.4$ ps to $\tau_{sd} \rightarrow \infty$, had very little effect on the “best-fit” value of the recoil alignment (rows 5-6 of Table I). Moreover, the choice of either a flat continuum background or a linear continuum background and the left-right margins of the fit region, had only minor effects on the “best-fit” value of the recoil alignment.

By contrast the presence of the 6978 keV background line had a significant impact on the least-squares-fit to the recoil alignment. The importance of including the 6978 keV line is demonstrated by comparing the results of fits performed with the 6978 keV peak included, which yielded $A_L^{stat} = 0.604 \pm 0.106$ (row 1), and the 6978 keV peak omitted, which yielded $A_L^{stat} = 0.426 \pm 0.078$ (row 8). In addition, we found a significant difference in “best fit” values of A_L^{stat} when comparing the cases of either (i) varying the 6978 keV line amplitude or (ii) fixing the 6978 keV line amplitude. In order to fix the amplitude of the 6978 keV $^{35}\text{Cl}(n, \gamma)$ line we used the amplitudes of the nearby 6678 keV and 7414 keV $^{35}\text{Cl}(n, \gamma)$ lines and their relative intensities taken from Krusche *et al* [34]. The free-amplitude fit gave a recoil alignment $A_L = 0.604 \pm 0.106$ with a 6978 keV peak amplitude $A^G = 89 \pm 30$ (row 1). By comparison the fixed-amplitude fit gave $A_L = 0.503 \pm 0.083$ with $A^G = 41$ (row 9), *i.e.* showing a difference of $\sim 1 \sigma$ for the recoil alignment and a discrepancy of $\sim 1.6 \sigma$ for the peak amplitude.

The 1.6σ discrepancy between the estimated amplitude and the fitted amplitude of the 6978 keV line may reflect the statistics of the 6978 keV background line, the presence of an unidentified background line, or the uncertainties in interpolating $^{35}\text{Cl}(n, \gamma)$ intensities. We consider the result of the free-amplitude fit to be most trustworthy.

In conclusion, by fitting the 7012 keV lineshape we obtained the recoil alignment $A_L^{stat} = 0.60 \pm 0.11$, which indicates the $^{14}\text{C}(2^+, 7012)$ recoil is highly orientated following muon capture. We found the alignment determination was relatively insensitive to the parameters related to the energy calibration, instrumental resolution, and slowing-down effects, but more sensitive to the presence of the 6978 keV $^{35}\text{Cl}(n, \gamma)$ background line.

IV. INTERPRETATION

A. Theoretical overview

The mass-14 system includes a well-known example of a highly suppressed allowed Gamow-Teller transition; the β -decay that connects the $^{14}\text{C}(0^+, 1)$ ground state and $^{14}\text{N}(1^+, 0)$ ground state. In lieu of g.s.-to-g.s. Gamow-Teller strength the $^{14}\text{N} \rightarrow ^{14}\text{C}$ GT strength is distributed across a few low-lying ^{14}C excited states, with most notable the 2^+ doublet at 7012 and 8318 keV [35]. Interestingly, the 2^+ doublet wavefunctions involve both $(0p)^{-2}$ components *and* $(0p)^{-4}(1s0d)^2$ components [36–38], with configuration mixing being indispensable to understanding the partitioning of the GT strength within the 2^+ doublet.

Calculations of the $\mu^- + ^{14}\text{N}(1^+, 0) \rightarrow \nu_\mu + ^{14}\text{C}(2^+, 7012)$ capture rate have been performed by Bukhvostov *et al.* [43], Mukhopadhyay [44,45], Kissener *et al.* [46], Desgrolard *et al.* [47,48] and Auerbach and Brown [49]. It is clearly established that a simple $(0p)^{-2}$ model for the $\mu^- + ^{14}\text{N}(1^+, 0) \rightarrow \nu_\mu + ^{14}\text{C}(2^+, 7012)$ transition over predicts the rate by roughly a factor of 5-10. As alluded to above, this discrepancy is understood as a result of the importance of the $(0p)^{-4}(1s0d)^2$ components in the $^{14}\text{C}(2^+, 7012)$ wavefunction, such configurations decreasing the wavefunction overlap between the ^{14}N initial state and the ^{14}C final state.

The longitudinal alignment of the ^{14}C recoil in the $^{14}\text{N}(1^+, 0) \rightarrow ^{14}\text{C}(2^+, 7012)$ transition has been studied theoretically by Bukhvostov and Popov [26,27] and Dmitrieva *et al.* [28].³ Bukhvostov and Popov [26,27] were first to advocate the alignment as a possible probe of the proton's induced pseudoscalar coupling g_p . Dmitrieva *et al.* [28] then extended this work to calculate both the recoil alignment and its hyperfine dependences using a $(0p)^2$ model space and including the forbidden nuclear matrix elements. For $g_p/g_a \simeq 7$ they obtained an alignment $A_L^{stat} \simeq 0.60$ when including the second-forbidden corrections and an alignment $A_L^{stat} \simeq 0.23$ when excluding the second-forbidden corrections, the authors tracing the striking contribution of forbidden terms to the operator $\mathbf{M}_{22} \cdot \sigma$. The possible effects of the $(0p)^{-4}(1s0d)^2$ components of the $^{14}\text{C}(2^+, 7012)$ wavefunction on the ^{14}C recoil alignment were however not considered in Refs. [26–28].

³Actually the authors give results for the γ -recoil angular correlation coefficient in the $^{14}\text{N}(1^+, 0) \rightarrow ^{14}\text{C}(2^+, 7012) \rightarrow ^{14}\text{C}(0^+, 0)$ sequence. However, as discussed in Appendix A, the γ -recoil correlation coefficient a_2 and recoil alignment A_L are related according to $a_2 = -\sqrt{\frac{5}{14}}A_L$ for $^{14}\text{N}(1^+, 0) \rightarrow ^{14}\text{C}(2^+, 7012) \rightarrow ^{14}\text{C}(0^+, 0)$.

B. Model calculations

Herein we have performed shell model calculations of the capture rate and the recoil alignment for the $^{14}\text{N}(1^+, 0) \rightarrow ^{14}\text{C}(2^+, 7012)$ transition in both a $(0p)^{-2}$ model space and a $(0p)^{-2} + (0p)^{-4}(1s0d)^2$ model space. For the $(0p)^{-2}$ calculation (denoted CKPOT) we used the $0p$ -shell effective interaction of Cohen and Kurath [50]. For the $(0p)^{-2} + (0p)^{-4}(1s0d)^2$ calculation we used the two-body matrix elements of: Cohen and Kurath [50] for the $0p$ shell interaction, Chung and Wildenthal [51] for the $1s0d$ shell interaction, and Millener and Kurath [52] for the cross-shell interactions (for further details see Warburton and Millener [53]). Moreover, we performed three versions of the $(0p)^{-2} + (0p)^{-4}(1s0d)^2$ calculation. In version one (denoted MK3CW1) the $1s0d$ single particle energies were fixed as given in Ref. [53]. In version two (denoted MK3CW2) the $1s-0d$ single particle energies were shifted by -3.0 MeV (from Ref. [53]) in order to reproduce the $\sim 50\%$ admixture of the $(0p)^{-4}(1s0d)^2$ configurations in the $^{14}\text{C}(2^+, 7012)$ wavefunction as determined in Refs. [36–38]. In version three (denoted MK3CW3) the $1s-0d$ single particle energies were shifted by -4.9 MeV (from Ref. [53]) in order to reproduce the $^{14}\text{N}(1^+, 0) \rightarrow ^{14}\text{C}(2^+, 7012)$ capture rate of $\Lambda^{stat} = (4.4 \pm 0.6) \times 10^3 \text{ s}^{-1}$ as quoted by Stocki *et al* [22].

We stress our goal was not to identify one particular model as preferable to another model. Rather, by different choices of valence nucleon spaces and single particle energies, we intended to expose the model dependences of the capture rate and the recoil alignment. In particular, by varying the $1s-0d$ single particle energies we changed the $(0p)^{-4}(1s0d)^2$ wavefunction admixture, the most obvious uncertainty in the nuclear structure of the 2^+ doublet.⁴ This permitted a better understanding of how the uncertainties in the $(0p)^{-4}(1s0d)^2$ admixture are mapped into the uncertainties in the capture rate Λ^{stat} and the recoil alignment A_L^{stat} .

A comparison of the excitation energies of the low-lying $(J^\pi, T) = (2^+, 1)$ states from the various models with the experimental data is given in Fig. 2. For CKPOT the single 2^+ state is very nearly pure $(1p_{3/2})^7(1p_{1/2})^3$. For MK3CW1 the lower-lying 2^+ state is dominantly $(1p_{3/2})^7(1p_{1/2})^3$ and the higher-lying 2^+ state is dominantly $(0p)^{-4}(1s0d)^2$. Neither CKPOT nor MK3CW1 are capable of reproducing either the small energy gap of the 2^+ doublet or the well-established mixing of the two 2^+ states. However, for MK3CW2 and MK3CW3, in which we adjusted by hand the splitting between the $0p$ shell and the $1s0d$ shell, the two lowest-lying 2^+ states are increasingly mixed, and the energy splitting of the 2^+ doublet is thus adequately reproduced. Note for MK3CW2 the $(0p)^{-4}(1s0d)^2$ admixture is $\sim 50\%$, this admixture dictating the choice of the single particle energies, while for MK3CW3 the $(0p)^{-4}(1s0d)^2$ admixture is $\sim 85\%$, this admixture reproducing the capture rate $\Lambda^{stat} = 4.4 \times 10^3 \text{ s}^{-1}$. Clearly, the energy splitting of the 2^+ doublet, the $(0p)^{-4}(1s0d)^2$ content of the 2^+ states, and the relative positions of the $0p$, $1s0d$ shells, are very strongly correlated.

In order to compute the capture rate and recoil alignment for $^{14}\text{N}(1^+, 0) \rightarrow ^{14}\text{C}(2^+, 7012)$

⁴The dependence of the $(0p)^{-4}(1s0d)^2$ wavefunction admixture on the $1s-0d$ single particle energies is a result of the proximity of the lowest-lying $(0p)^{-2}$ and $(0p)^{-4}(1s0d)^2$ configurations with spin-parity 2^+ . This circumstance implies a large mixing between $(0p)^{-2}$ configurations and $(0p)^{-4}(1s0d)^2$ configurations in the 2^+ doublet.

we employed the formalism of Walecka [55]. For completeness we give in Appendix B the details of our model calculations of the recoil alignment. We took the weak nuclear current as a sum of A one-body nucleonic currents, *i.e.* ignoring the effects of exchange currents, isobar excitations, etc. The required nuclear matrix elements were computed with one-body transition densities obtained from the OXBASH shell model code [56] and with harmonic oscillator radial wavefunctions and an oscillator parameter $b = 1.7$ fm. We set the weak vector coupling $g_v = 1$ and the weak magnetic coupling $g_M = 3.706$, and assumed the induced scalar coupling g_s and induced tensor couplings g_t were zero. In order to scale the weak vector and magnetic couplings to finite q^2 we assumed a dipole form factor with $\Lambda^2 = 0.73$ GeV². The three-momentum transfer $q = 97$ MeV/ c was computed via energy-momentum conservation

$$q + q^2/2M_t = m_\mu - \Delta E - \epsilon_b \quad (3)$$

where M_t is the target mass, ΔE is the $^{14}\text{N}-^{14}\text{C}^*$ nuclear binding energy difference, and ϵ_b is the muon binding energy. The muon wavefunction was assumed to be constant over the nucleus, with a reduction factor $R = 0.84$ accounting for the difference between a point nucleus and a finite nucleus (for details see Ref. [55]).

Lastly, to assist our later discussions of model dependences, we make a few comments on the model calculations. We remind the reader a $1^+ \rightarrow 2^+$ transition involves three multipoles $J^\pi = 1^+, 2^+, 3^+$, although for $^{14}\text{N}(1^+, 0) \rightarrow ^{14}\text{C}(2^+, 7012)$ the contribution from $J^\pi = 3^+$ terms are very small. The $J^\pi = 1^+, 2^+$ multipoles involve four independent amplitudes ($\mathcal{L}_1^5 - \mathcal{M}_1^5$, $\mathcal{T}_1^{el5} - \mathcal{T}_1^{mag}$, $\mathcal{L}_2 - \mathcal{M}_2$, $\mathcal{T}_2^{el} - \mathcal{T}_2^{mag5}$) which themselves are products of basic multipole operators and weak coupling constants. For $J^\pi = 1^+, 2^+$ the multipole operators are the allowed Gamow-Teller operator $\mathbf{M}_{10} \cdot \sigma$, second-forbidden Gamow-Teller operators $\mathbf{M}_{12} \cdot \sigma$ and $\mathbf{M}_{22} \cdot \sigma$, and momentum-dependent contributions $\mathbf{M}_{11} \cdot \nabla$, $\mathbf{M}_{21} \cdot \nabla$, $\mathbf{M}_{23} \cdot \nabla$ and $\mathbf{M}_1 \sigma \cdot \nabla$. The capture rate, recoil alignment and other observables in $^{14}\text{N}(1^+, 0) \rightarrow ^{14}\text{C}(2^+, 7012)$ are all combinations of the nuclear matrix elements of these basic multiple operators and the weak coupling constants. For further details see Walecka [55], Donnelly and Haxton [57] and Appendix B.

C. Capture rate results

The $\mu^- + ^{14}\text{N}(1^+, 0) \rightarrow \nu_\mu + ^{14}\text{C}(1^+, 7012)$ capture rate for a statistical mixture of the hyperfine states, has been measured by Babaev *et al.* [39], Thompson *et al.* [40], Belotti *et al.* [41], Giffon *et al.* [42] and Stocki *et al.* [22]. Unfortunately, the experimental results have significant scatter, with rates as small as $(2.2 \pm 0.9) \times 10^3$ s⁻¹ [22] and as large as $(10 \pm 3) \times 10^3$ s⁻¹ [39]. Stocki *et al.* have quoted a world average of $\Lambda^{stat} = (4.4 \pm 0.6) \times 10^3$ s⁻¹ [22].

Our results from the model calculations of the muon capture rate and its hyperfine dependence in the $^{14}\text{N}(1^+, 0) \rightarrow ^{14}\text{C}(2^+, 7012)$ transition are listed in Table II. Also given in Table II are the $(0p)^{-4}(1s0d)^2$ admixture in the ^{14}C final state and the dominant $0p_{3/2} \rightarrow 0p_{1/2}$ one-body transition density for the $^{14}\text{N} \rightarrow ^{14}\text{C}$ transition. Note that for $^{14}\text{N}(1^+, 0) \rightarrow ^{14}\text{C}(2^+, 7012)$ the $F = 3/2$ capture rate and statistical capture rate are overwhelmingly determined by the product of the Gamow-Teller matrix element $\mathbf{M}_{10} \cdot \sigma$ and the weak axial coupling g_a . Moreover, as shown in Fig. 3, the capture rate is a strong function of the $(0p)^{-4}(1s0d)^2$ content of

the ^{14}C nuclear wavefunction, the rate reflecting the decreasing wavefunction overlap with increasing $(0p)^{-4}(1s0d)^2$ admixture.

As found in earlier investigations the simple $0p$ -shell grossly over-estimates the $^{14}\text{N}(1^+, 0) \rightarrow ^{14}\text{C}(1^+, 7012)$ capture rate. Clearly, increasing the $2\hbar\omega$ admixture by simply changing the $0p$, $1s$ - $0d$ shell splitting is capable of eliminating the discrepancy between experiment and theory – although this procedure is rather ad hoc.

D. Recoil alignment results

Our results for the model calculations of the recoil alignment in the $^{14}\text{N}(1^+, 0) \rightarrow ^{14}\text{C}(2^+, 7012)$ transition are plotted in Fig. 4. Note that Fig. 4 shows the recoil alignment for a statistical mixture of the hyperfine states, as determined by experiment and discussed in Sec. III. The alignment A_L^{stat} of the statistical mixture was obtained from the two alignments A_L^\pm of the hyperfine states via

$$A_L^{stat} = \frac{f_+ A_L^+ + f_- A_L^- R}{f_+ + f_- R} \quad (4)$$

where f_+ , f_- are the statistical populations of the hyperfine states and $R = \Lambda_-/\Lambda_+$ is the hyperfine dependence of the capture rate. Therefore, in principle, the alignment A_L^{stat} is a function of the hyperfine alignments A_L^\pm and the capture rates Λ^\pm , although, in practice, as R is small one finds the alignment is approximately $A_L^{stat} \simeq A_L^+$.

A useful comparison for the model calculations of the recoil alignment is the Fujii-Primakoff approximation [58]. In the Fujii-Primakoff approximation the $\mathbf{M}_{10} \cdot \sigma$ matrix element is retained while the forbidden matrix elements are omitted. The approximation yields

$$A_L^+ = +\sqrt{14}(-X^2 - X + 2)/(+4 + 2X + 5) \quad (5)$$

$$A_L^- = -\sqrt{\frac{7}{10}} \quad (6)$$

where the quantity $X = (G_A - G_P)/G_A$ and the effective coupling constants are $G_A = -(g_a + (q/2M)(g_v + g_m))$ and $G_P = -(q/2M)(g_p - g_a + g_v + g_m)$. With $g_v = 1.00$, $g_m = 3.706$ and $q \sim 100$ MeV/c one obtains a value of $A_L^+ \simeq +0.12$ for $g_p/g_a \simeq 0$ and $A_L^+ \simeq +0.35$ for $g_p/g_a \simeq 7$, thus indicating the importance of the induced coupling on the recoil alignment.

For $g_p/g_a = 6.7$ the model results of Fig. 4 give recoil alignments that range from $A_L^{stat} = +0.45$ (MK3CW3) to $A_L^{stat} = +0.53$ (CKPOT). The relatively small model dependence of the alignment may be contrasted with the relatively large model dependence of the capture rate, it decreasing by roughly a factor of five from CKPOT to MK3CW3 (see Table II). To better understand this striking difference in model sensitivities between A_L^{stat} and Λ^{stat} we remind the reader the alignment is governed by ratios of nuclear matrix elements and weak coupling constants. Therefore, as both the numerator and denominator in A_L^{stat} are dominated by $\mathbf{M}_{10} \cdot \sigma$, the recoil alignment A_L^{stat} is rather weakly model dependent although the matrix element $\mathbf{M}_{10} \cdot \sigma$ itself is rather strongly model dependent. The residual model dependence of the recoil alignment A_L^{stat} may be ultimately traced to the small contributions of the $1s$ - $0d$ one-body transitions densities to the $^{14}\text{N}(1^+, 0) \rightarrow ^{14}\text{C}(2^+, 7012)$ transition.

In Fig. 5 we show the relative contributions of the different matrix elements to the recoil alignment A_L^{stat} . The plot reveals a substantial contribution from the $\ell = 2$ Gamow-Teller matrix elements (*e.g.* $\mathbf{M}_{22} \cdot \sigma$) and a significant contribution from the axial charge matrix element (*i.e.* $\mathbf{M}_{10} \sigma \cdot \nabla$). The effects of other $J = 2$ matrix elements are small and the effects of the $J = 3$ matrix elements are negligible. Consequently, the dominant source of model dependences in computing A_L^{stat} is the knowledge of the ratio between the $\ell = 2$ GT matrix elements and the $\mathbf{M}_{10} \cdot \sigma$ matrix element. This ratio is sensitive to the $(0p)^{-4}(1s0d)^2$ wavefunction admixture through the $1s-0d$ one-body transition densities.

E. Coupling constant sensitivity

Our alignment measurement, $A_L^{stat} = 0.60 \pm 0.11$, and alignment calculation, $A_L^{stat} = 0.45 - 0.53$, are clearly in reasonable agreement. Indeed the comparison between model and data is sufficient to constrain the coupling's value to $g_p/g_a \geq 5$ (CKPOT) to $g_p/g_a \geq 9$ (MK3CW3). Our bound on g_p/g_a is consistent with the results from the ^{12}C recoil polarization experiments, which yielded $g_p/g_a = 9.8 \pm 1.8$, but inconsistent with the results from the ^{28}Si recoil alignment experiments, which yielded $g_p/g_a = 1.0_{-1.2}^{+1.1}$. Our result is also consistent with the prediction $g_p/g_a = 6.7$ of chiral symmetry arguments [2,3].

In considering the dependence of A_L^{stat} on g_p its helpful to summarize the terms that contribute to A_L^{stat} (for definiteness we employ the MK3CW3 model). In the limit of (i) no forbidden nuclear matrix elements and (ii) no induced pseudoscalar coupling, the recoil alignment is $A_L^{stat} \simeq 0.09$. The contribution of the coupling $g_p = 6.7g_a$ increases the recoil alignment to $A_L^{stat} \simeq 0.25$ and the contribution of $\ell = 2$ GT terms increase the recoil alignment to $A_L^{stat} \simeq 0.40$. Finally the remaining nuclear matrix elements, mostly the axial charge matrix element, are responsible for increasing the value to $A_L^{stat} \simeq 0.45$. Clearly the agreement of model and data for A_L^{stat} lend support to significant contributions from both the induced pseudoscalar coupling and the $\ell = 2$ forbidden corrections.

V. SUMMARY

In summary, we report a measurement of the longitudinal alignment A_L^{stat} of the recoil nucleus in the $^{14}\text{N}(1^+, 0) \rightarrow ^{14}\text{C}(2^+, 7012)$ transition. The alignment was determined from the Doppler lineshape of the 7012 keV gamma-ray from the $^{14}\text{C}(2^+, 7012) \rightarrow ^{14}\text{C}(0^+, 0)$ transition, *i.e.* using the method of Grenacs *et al.* [23]. Our result of $A_L^{stat} = 0.60 \pm 0.11$ indicates a large, positive alignment of the ^{14}C recoil nucleus originating from the $V-A$ structure of the weak interaction.

In addition, we report new calculations of the capture rate and the recoil alignment for the $^{14}\text{N}(1^+, 0) \rightarrow ^{14}\text{C}(2^+, 7012)$ transition. The calculations were conducted in both a simple $0p^{-2}$ model space and a richer $0p^{-2} + 0p^{-4}(1s0d)^2$ model space. As discussed by others, the capture rate Λ^{stat} is dominated by the $\ell = 0$ Gamow-Teller matrix element and the weak axial coupling g_a , and is highly sensitive to the $(0p)^{-4}(1s0d)^2$ admixture in the $^{12}\text{C}(2^+, 7012)$ wavefunction. By comparison, we found the recoil alignment A_L^{stat} has substantial contributions from the induced pseudoscalar coupling and the second-forbidden Gamow-Teller matrix

elements. Interestingly, the recoil alignment is comparatively insensitive to the $(0p)^{-4}(1s0d)^2$ components of the $^{12}\text{C}(2^+, 7012)$ wavefunction.

Our measured alignment of $A_L^{stat} = 0.60 \pm 0.11$ and calculated alignments of $A_L^{stat} = 0.45\text{--}0.53$ are in reasonable agreement. We view this reasonable agreement as evidence supporting the model estimates for the contributions of the induced pseudoscalar coupling and the second-forbidden corrections to the ^{14}C recoil alignment. Indeed, by comparing the model calculations and experimental data, we derived a bound on g_p that ranges from $g_p/g_a \geq 9$ for the MK3CW3 calculation to $g_p/g_a \geq 5$ for the CKPOT calculation. This bound is consistent with the value $g_p/g_a = 9.8 \pm 1.8$ obtained from the determination of the $^{12}\text{C}(0^+, 0) \rightarrow ^{12}\text{B}(1^+, 0)$ transition recoil polarization, but inconsistent with the value $g_p/g_a = 1.0_{-1.2}^{+1.1}$ obtained from the determination of the $^{28}\text{Si}(0^+, 0) \rightarrow ^{28}\text{Al}(1^+, 2201)$ recoil alignment. Our result is consistent with $g_p/g_a = 6.7$ – the theoretical prediction derived from chiral symmetry arguments.

Our experiment was limited by both the statistical accuracy of the Doppler lineshape and the unfortunate presence of the $^{35}\text{Cl}(n, \gamma)$ 6978 keV background line. The model uncertainties are apparently dominated by the uncertainties in the $\ell = 2$ Gamow-Teller matrix elements arising from the uncertainties in the $(0p)^{-4}(1s0d)^2$ wavefunction admixture. We suggest, with better statistics and reduced backgrounds, the $^{14}\text{N}(1^+, 0) \rightarrow ^{14}\text{C}(2^+, 7012)$ transition would offer a competitive window on induced currents and forbidden contributions in muon capture.

We wish to thank Drs. Ermias Gete, David Measday, Belal Moftah and Michael Saliba for assistance in collecting the data and the TRIUMF technical staff for the operation of the TRIUMF cyclotron. We also acknowledge both the National Science Foundation (USA) and the Natural Sciences and Engineering Research Council (Canada) for their financial support.

APPENDIX A: RELATION BETWEEN THE γ - ν CORRELATION AND THE LONGITUDINAL ALIGNMENT

Herein we consider the sequence $\mu^- + {}^{14}\text{N}(1^+, 0) \rightarrow \nu_\mu + {}^{14}\text{C}(2^+, 7012) \rightarrow \gamma + {}^{14}\text{C}(0^+, 0)$ which involves an allowed Gamow-Teller ($1^+ \rightarrow 2^+$) transition and pure electric quadrupole ($2^+ \rightarrow 0^+$) decay. We denote the initial, intermediate and final state angular momenta by J_1 , J_2 and J_3 , the neutrino and photon directions by $\hat{\nu}$ and \hat{k} , and the γ -ray multipolarity by L^π . For either unpolarized muons, $\vec{P}_\mu = 0$, or perpendicular geometry, $\vec{P}_\mu \cdot \hat{k} = 0$, the γ - ν directional correlation is given by [26–29]

$$W(\theta) = 1 + \sum_s a_s P_s(\cos \theta) \quad (\text{A1})$$

where $P_s(\cos \theta)$ are the Legendre polynomials, a_s are the γ - ν correlation coefficients, and $\cos \theta = \hat{\nu} \cdot \hat{k}$. In Eqn. A1 the summation involves even Legendre polynomials, and is bounded by the smaller of $2J_2$ or $2L$. Thus for ${}^{14}\text{N}(1^+, 0) \rightarrow {}^{14}\text{C}(2^+, 7012) \rightarrow {}^{14}\text{C}(0^+, 0)$ the permissible values are $s = 2$ and $s = 4$.

The γ - ν correlation coefficients a_s are functions of both the μ capture process and γ -decay process. More specifically the coefficients a_s are given by

$$a_s = A_s B_s \quad (\text{A2})$$

where A_s is dictated by the $\mu^- + {}^{14}\text{N}(1^+, g.s.) \rightarrow \nu_\mu + {}^{14}\text{C}(2^+, 7012)$ transition, and B_s is dictated by the ${}^{14}\text{C}(2^+, 7012) \rightarrow \gamma + {}^{14}\text{C}(0^+, 0)$ transition. The quantity A_s is the rank- s orientation of the recoil nucleus J_2 about the neutrino axis $\hat{\nu}$. The quantity B_s is governed by the spin-parity sequence $J_2 \rightarrow J_3$ and the multipolarity L^π (a useful reference that contains tabulations of B_s coefficients is Ciechanowicz and Oziewicz [29]). For $2^+ \rightarrow 0^+$ transitions one finds that $B_2 = -\sqrt{\frac{5}{14}}$ and $B_4 = -\sqrt{\frac{8}{7}}$.

Our model calculations for $\mu^- + {}^{14}\text{N}(1^+, 0) \rightarrow \nu_\mu + {}^{14}\text{C}(2^+, 7012) \rightarrow \gamma + {}^{14}\text{C}(0^+, 0)$ have shown the role of the rank-4 orientation in the γ - ν correlation may be safely ignored. For the rank-2 orientation we have herein denoted A_2 as the recoil's longitudinal alignment $A_L \equiv A_2$. The relationship between the γ - ν directional correlation coefficient a_2 and the recoil longitudinal alignment A_L is thus simply $a_2 = -\sqrt{\frac{5}{14}} A_L$.

APPENDIX B: MODEL CALCULATIONS OF THE LONGITUDINAL ALIGNMENT

One approach in addressing the various physical observables in nuclear muon capture is the helicity representation. In the helicity representation one views capture as the two-body decay of a spin- F muonic atom into a left-handed muon neutrino and a spin- J_f recoil nucleus. The rank- s orientation A_s^F of the recoil nucleus about the neutrino axis is

$$A_s^F = (-1)^s \sqrt{2s+1} \sum_\lambda \langle J_f \lambda s 0 | J_f \lambda \rangle |T_\lambda^F|^2 / \sum_\lambda |T_\lambda^F|^2 \quad (\text{B1})$$

where F is the muonic atom hyperfine state, λ is the recoil nucleus helicity state, and T_λ^F are the contributing helicity amplitudes [58,55,29].

For $\mu^- + {}^{14}\text{N}(1^+, 0) \rightarrow \nu_\mu + {}^{14}\text{C}(2^+, 7012)$ the initial hyperfine states are $F = J_i \pm 1/2 = 1/2, 3/2$. Thus according to Eqn. B1, the various observables in $F_- = 1/2$ capture are determined by two helicity amplitudes, *i.e.* $T_{-1}^{1/2}, T_0^{1/2}$, and in $F_+ = 3/2$ capture are determined by four helicity amplitudes, *i.e.* $T_{-2}^{3/2}, T_{-1}^{3/2}, T_0^{3/2}, T_{+1}^{3/2}$. These six amplitudes contain all the dependences on the weak couplings and the nuclear structure in the $\mu^- + {}^{14}\text{N}(1^+, 0) \rightarrow \nu_\mu + {}^{14}\text{C}(2^+, 7012)$ transition.

More convenient for model calculations than the helicity amplitudes T_λ^F are the electroweak amplitudes denoted $\mathcal{L}_J - \mathcal{M}_J$ and $\mathcal{T}_J^{el} - \mathcal{T}_J^{mag}$ where $\mathcal{M}_J, \mathcal{L}_J, \mathcal{T}_J^{el}$ and \mathcal{T}_J^{mag} represent the charge, longitudinal, transverse electric and transverse magnetic operators. For $\mu^- + {}^{14}\text{N}(1^+, g.s.) \rightarrow \nu_\mu + {}^{14}\text{C}(2^+, 7012)$ there are six electroweak amplitudes corresponding to the three multipolarities $J^\pi = 1^+, 2^+, 3^+$ where $\mathcal{L}_J - \mathcal{M}_J$ and $\mathcal{T}_J^{el} - \mathcal{T}_J^{mag}$ are simple products of basic multipole operators and weak coupling constants [55,57] (the specific relations between the electroweak amplitudes and the helicity amplitudes are given in Refs. [29]). For $\mu^- + {}^{14}\text{N}(1^+, 0) \rightarrow \nu_\mu + {}^{14}\text{C}(2^+, 7012)$ the relevant formulas for $\mathcal{L}_J - \mathcal{M}_J$ and $\mathcal{T}_J^{el} - \mathcal{T}_J^{mag}$ with multipolarities $J^\pi = 1^+, 2^+$ are reproduced in Table III. They involve the allowed Gamow-Teller operator $\mathbf{M}_{10} \cdot \sigma$, the second forbidden Gamow-Teller operators $\mathbf{M}_{12} \cdot \sigma$ and $\mathbf{M}_{22} \cdot \sigma$, and the momentum-dependent operators $\mathbf{M}_1 \sigma \cdot \nabla, \mathbf{M}_{11} \cdot \nabla, \mathbf{M}_{21} \cdot \nabla$ and $\mathbf{M}_{23} \cdot \nabla$. The contributions from $J^\pi = 3^+$ terms to $\mu^- + {}^{14}\text{N}(1^+, 0) \rightarrow \nu_\mu + {}^{14}\text{C}(2^+, 7012)$ are very small.

Finally, the required multi-particle weak matrix elements $\langle J_f || O^J || J_i \rangle$, between an initial many-body state $|J_i \rangle$ and final many-body state $|J_f \rangle$, were obtained from single-particle weak matrix elements $\langle \alpha' || O^J || \alpha \rangle$, between an initial single-particle state $|\alpha \rangle \equiv |n, j, \ell \rangle$ and final single-particle state $|\alpha' \rangle \equiv |n', j', \ell' \rangle$, via [57]

$$\langle J_f || O^J || J_i \rangle = \sum_{\alpha, \alpha'} C(J, \alpha, \alpha', J_f, J_i) \langle \alpha' || O^J || \alpha \rangle \quad (\text{B2})$$

where O^J denotes the relevant operator and $C(J, \alpha, \alpha', J_f, J_i)$ denotes the so-called one-body transition densities. The one-body transition densities govern the contributions of the various single-particle matrix element $\langle \alpha' || O^J || \alpha \rangle$ to the multi-particle matrix element $\langle J_f || O^J || J_i \rangle$.

TABLES

TABLE I. Summary of fits to the 7012 keV γ -ray lineshape from the $^{14}\text{N}(0, 1^+) \rightarrow ^{14}\text{C}(7012, 2^+)$ transition. A_G is the amplitude of the 6978 keV background peak, X^D is the position of the 7012 KeV Doppler peak, σ is the instrumental resolution, and τ_{sd} is the slowing-down time. We also distinguish between the fits with a flat continuum background (denoted 1 par.) and a linear continuum background (denoted 2 par.). The resulting “best-fit” values for A_L^{stat} are listed in the last column.

A^G	X^D	$\sigma^{G/D}$	τ_{sd}	ΔE	Bkgd.	A_L
free	free	0.82	0.011	0.00747	2 par.	0.604 ± 0.106
free	7012	0.82	0.011	0.00747	2 par.	0.610 ± 0.092
free	free	1.08	0.011	0.00747	2 par.	0.617 ± 0.115
free	free	0.66	0.011	0.00747	2 par.	0.592 ± 0.095
free	free	0.82	0.000	0.00747	2 par.	0.632 ± 0.104
free	free	0.82	0.022	0.00747	2 par.	0.578 ± 0.105
free	free	0.82	0.011	0.00747	1 par.	0.605 ± 0.100
0	free	0.82	0.011	0.00747	2 par.	0.426 ± 0.078
41	free	0.82	0.011	0.00747	2 par.	0.503 ± 0.083

TABLE II. Results of the model calculations for the capture rate and its hyperfine dependence for the $^{14}\text{N}(1^+, 0) \rightarrow ^{14}\text{C}(2^+, 7012)$ transition. The hyperfine capture rates are denoted Λ^\pm and the statistical capture rate is denoted Λ^{stat} . Also given for the different models are the $0p_{3/2} \rightarrow 0p_{1/2}$ one-body transition density (column five) and the $0p^{-4}1s0d^2$ wavefunction admixture (column six).

Model	Λ_+	Λ_-	Λ^{stat}	Λ_-/Λ_+	$0p_{3/2} \rightarrow 0p_{1/2}$	4h-2p
CKPOT	24.8×10^3	1.0×10^3	16.9×10^3	0.040	1.100	0%
MK3CW1	23.8×10^3	1.3×10^3	16.3×10^3	0.053	1.005	$\sim 20\%$
MK3CW2	18.3×10^3	1.1×10^3	12.6×10^3	0.058	0.808	$\sim 50\%$
MK3CW3	6.3×10^3	0.42×10^3	4.3×10^3	0.067	0.362	$\sim 85\%$

TABLE III. Decomposition of the electroweak operators $\mathcal{L}_J - \mathcal{M}_J$ and $\mathcal{T}_J^{el} - \mathcal{T}_J^{mag}$ with multiplicities $J^\pi = 1^+, 2^+$ into the basic multipole operators and the weak coupling constants. The basic multipole operators M_J , $\mathbf{M}_{JL} \cdot \boldsymbol{\sigma}$, $\mathbf{M}_{JL} \cdot \boldsymbol{\nabla}$ and $M_J \boldsymbol{\sigma} \cdot \boldsymbol{\nabla}$ are discussed in the Appendix B.

J^π	electroweak operator	multipole operator decomposition
1^+	$L_1^5 - M_1^5$	$i[(g_a + \frac{q}{2M}(g_a - g_p))(\sqrt{\frac{1}{3}}\mathbf{M}_{10} \cdot \boldsymbol{\sigma} + \sqrt{\frac{2}{3}}\mathbf{M}_{12} \cdot \boldsymbol{\sigma}) + \frac{q}{M}g_a M_1 \boldsymbol{\sigma} \cdot \boldsymbol{\nabla}] \tau^\pm$
1^+	$T_1^{el5} - T_1^{mag}$	$i[(g_a - \frac{q}{2M}(g_v - g_m))(\sqrt{\frac{2}{3}}\mathbf{M}_{10} \cdot \boldsymbol{\sigma} - \sqrt{\frac{1}{3}}\mathbf{M}_{12} \cdot \boldsymbol{\sigma}) + \frac{q}{M}g_v \mathbf{M}_{11} \cdot \boldsymbol{\nabla}] \tau^\pm$
2^+	$L_2 - M_2$	$-g_v M_2 \tau^\pm$
2^+	$T_2^{el} - T_2^{mag5}$	$i[(-g_a + \frac{q}{2M}(g_v + g_m))\mathbf{M}_{22} \cdot \boldsymbol{\sigma} + \frac{q}{M}g_v(\sqrt{\frac{3}{5}}\mathbf{M}_{21} \cdot \boldsymbol{\nabla} - \sqrt{\frac{2}{5}}\mathbf{M}_{23} \cdot \boldsymbol{\nabla})] \tau^\pm$

FIGURES

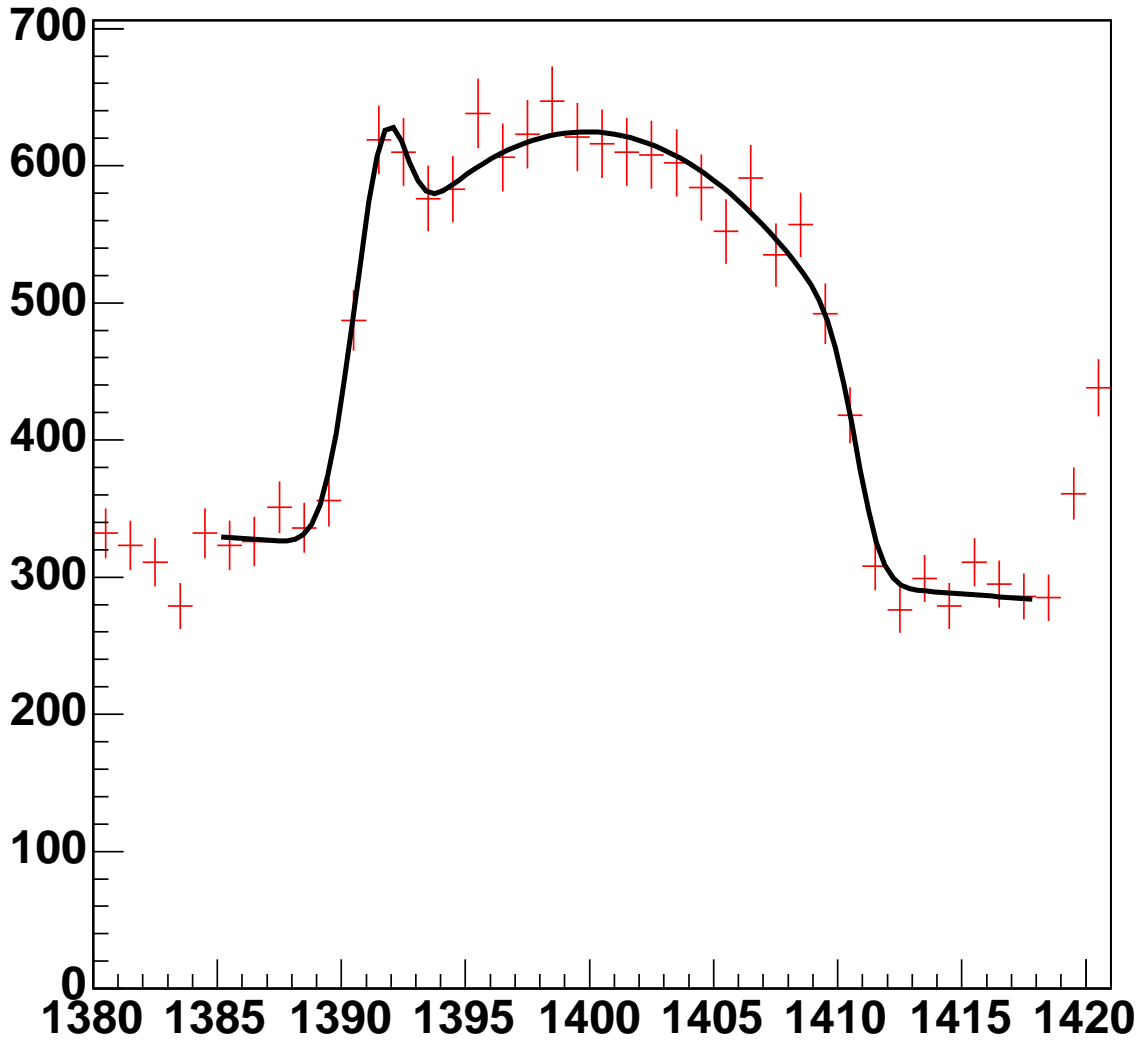


FIG. 1. The Doppler lineshape of the 7012 keV gamma-ray from the $\mu^- + {}^{14}\text{N}(1^+, 0) \rightarrow \nu_\mu + {}^{14}\text{C}(2^+, 7012) \rightarrow \gamma + {}^{14}\text{C}(0^+, 0)$ sequence. The rounded top of the 7012 keV lineshape is a reflection of the ${}^{14}\text{C}$ recoil alignment in the μ capture process. The small peak on the far lefthand side of the Doppler lineshape is the 6978 keV background line. The solid line is the benchmark fit to the Doppler lineshape (see text for details).

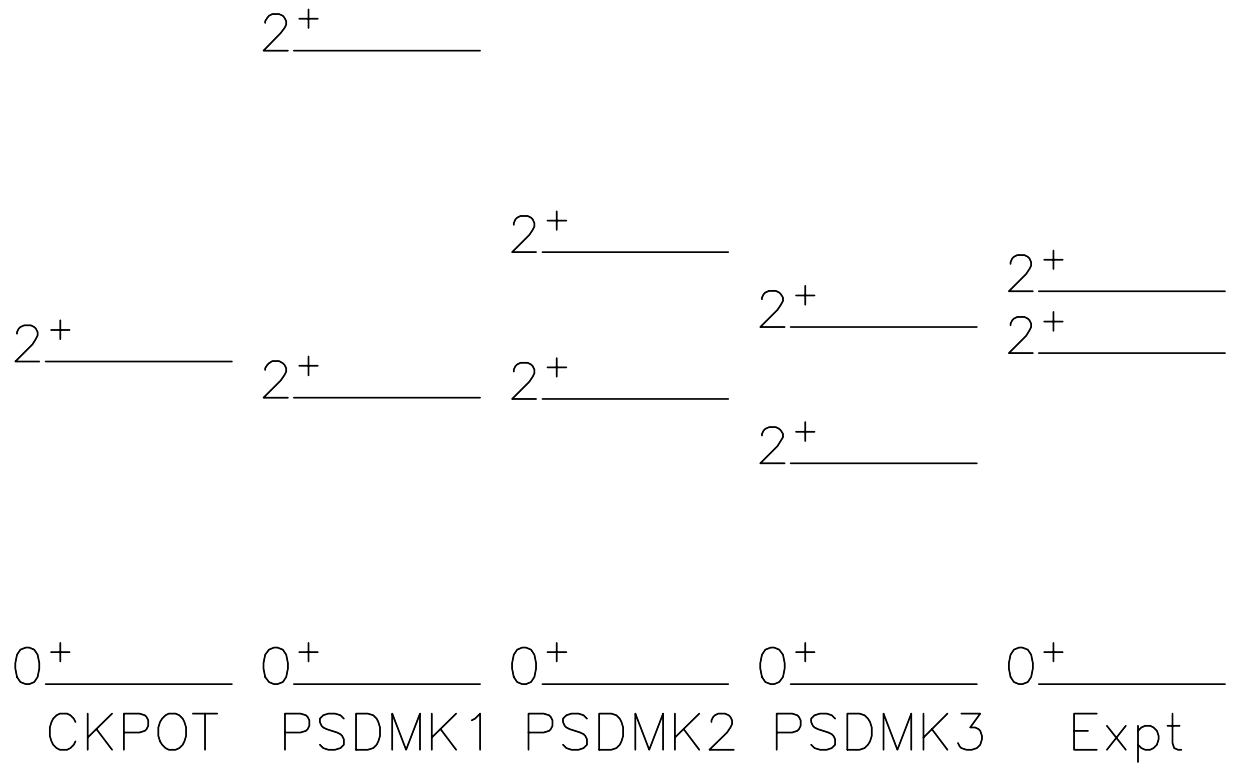


FIG. 2. Energy levels of the low-lying 2^+ states from the experimental data and the model calculations. The experimental excitation energies of the first and second 2^+ states are respectively 7012 and 8318 keV. The $2\hbar\omega$ admixture in the lowest-lying 2^+ state of the three MK3CW calculations is increasing from left to right.

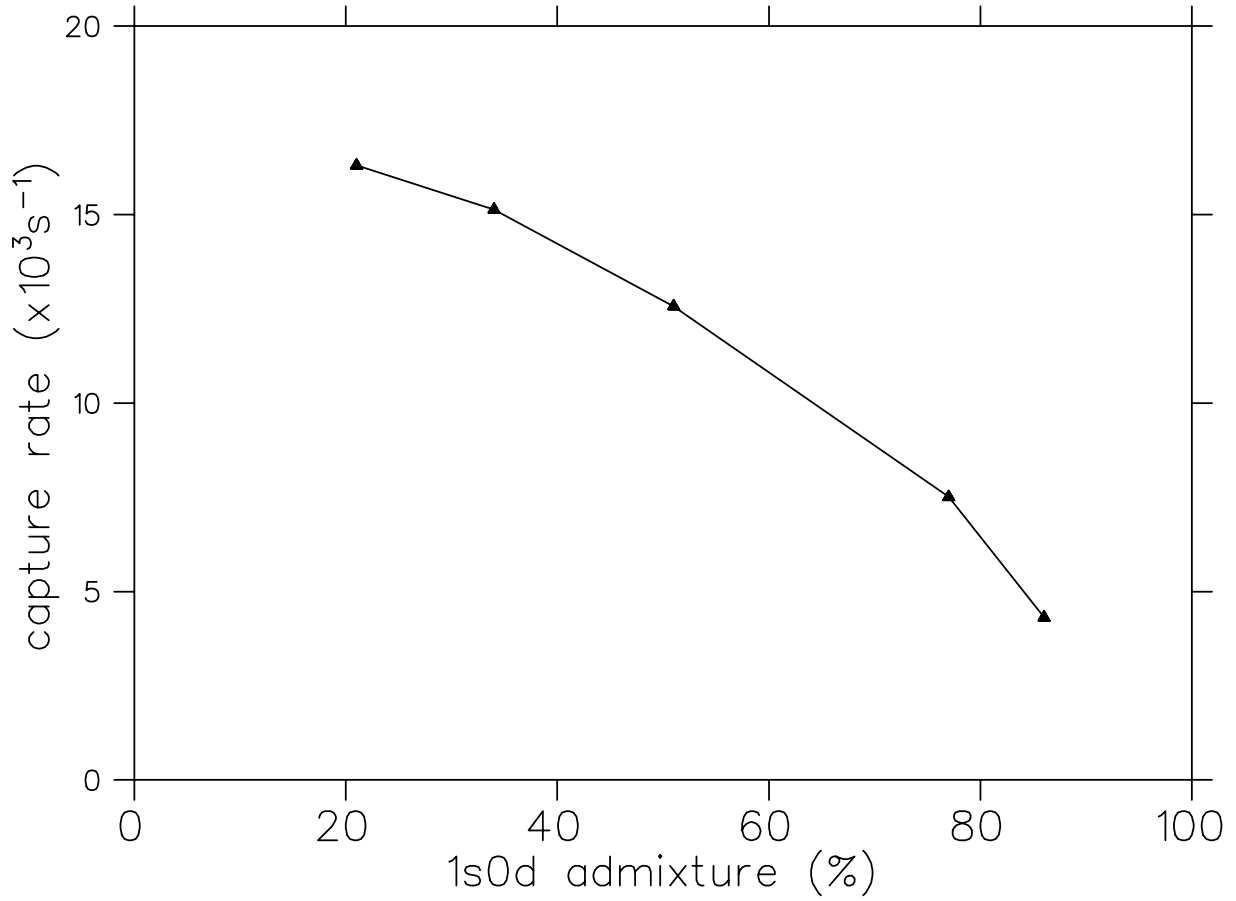


FIG. 3. The statistical capture rate for $\mu^- + {}^{14}\text{N}(1^+, g.s.) \rightarrow \nu_\mu + {}^{14}\text{C}(2^+, 7012)$ as a function of the $(0p)^{-4}(1s0d)^2$ wavefunction admixture. The calculations were performed by varying the energy separation between the $0p$ shell and the $1s0d$ shell in the MK3CW model calculations.

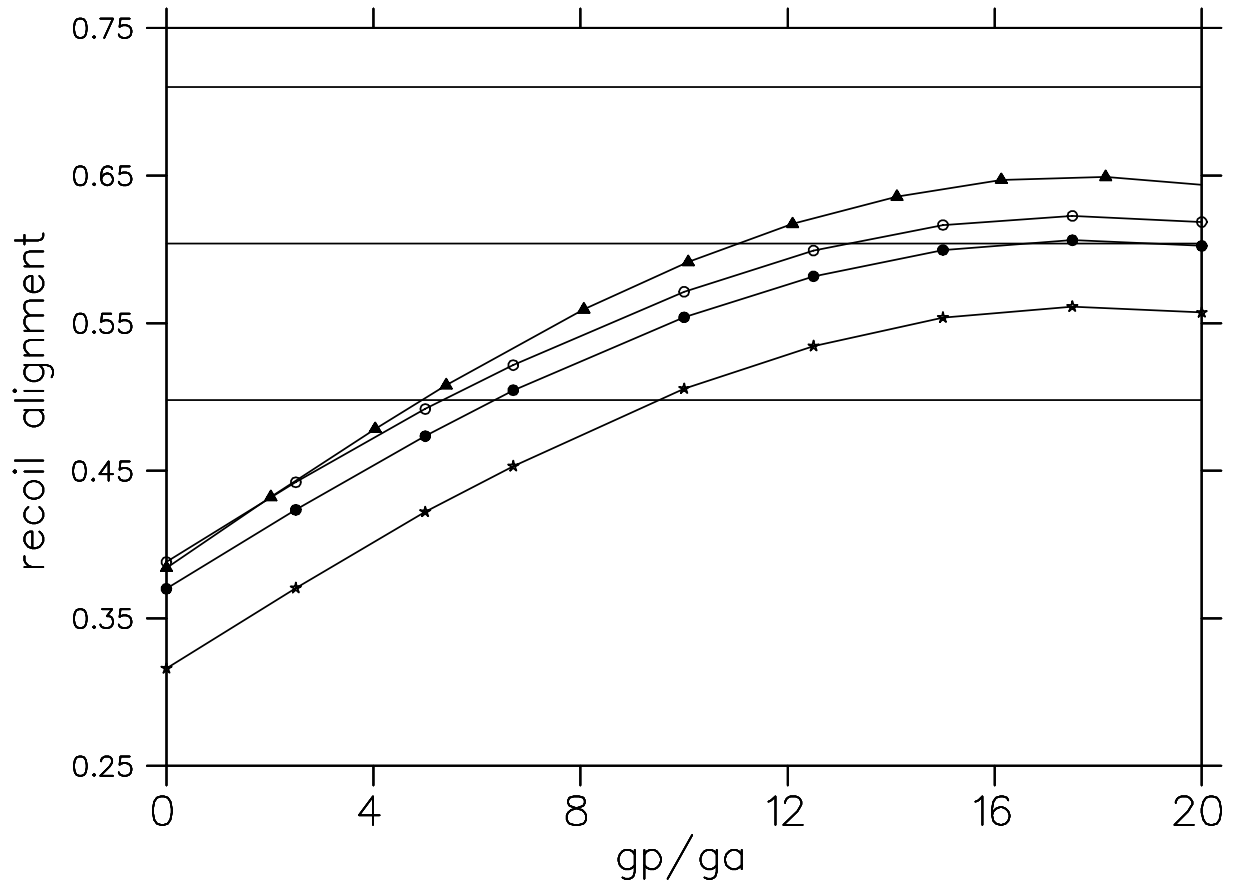


FIG. 4. The recoil alignment of the ^{14}C recoil as a function of the coupling constant ratio g_p/g_a . The calculations were performed for CKPOT (diamonds), MK3CW1 (open circles), MK3CW2 (filled circles), and MK3CW3 (stars). The horizontal lines indicate the central value and error bar for the experimental result $A_L^{stat} = 0.60 \pm 0.11$.

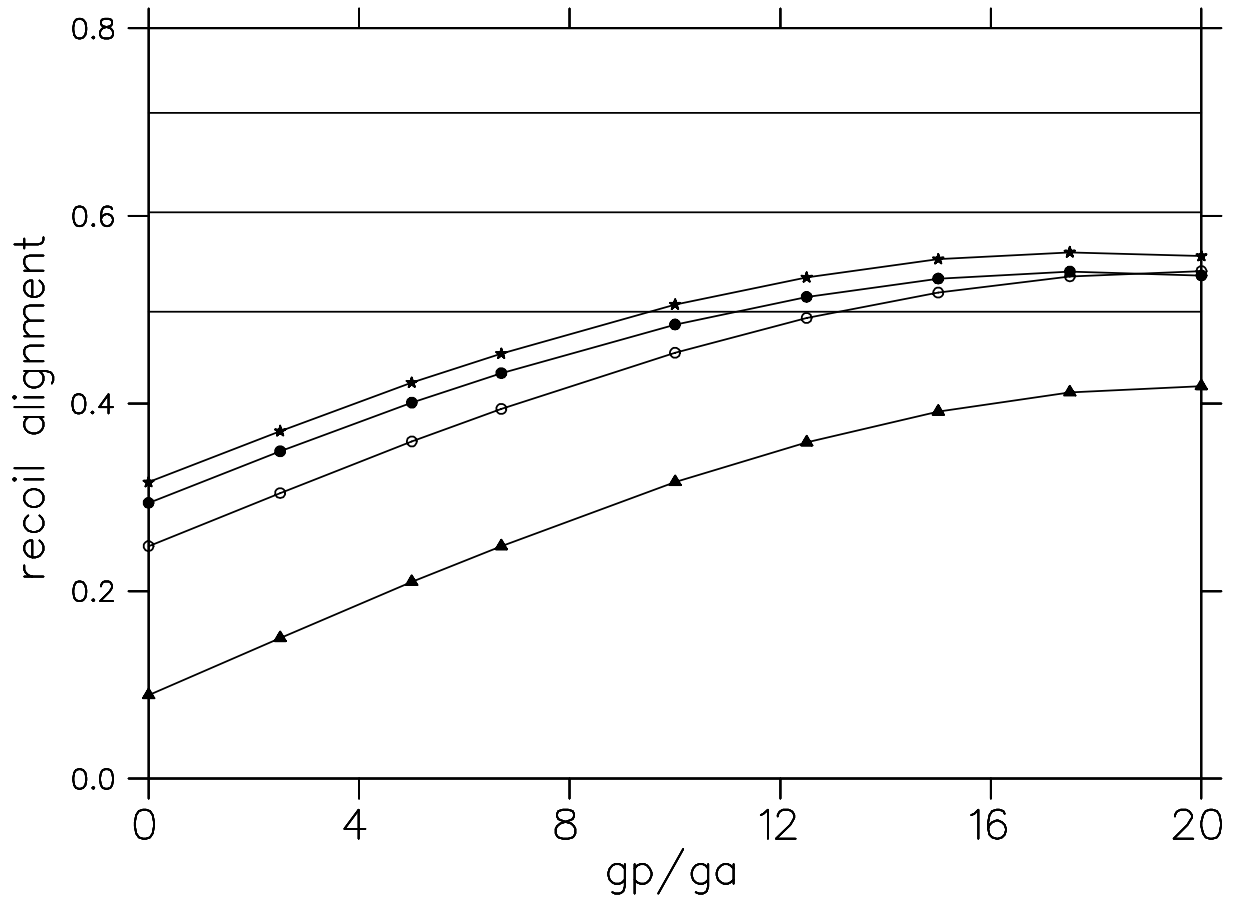


FIG. 5. The recoil alignment of the ^{14}C recoil as a function of the coupling constant ratio g_p/g_a . The calculations were performed with MK3CW3 for $M_{10} \cdot \sigma$ only (diamonds), for $M_{10} \cdot \sigma$ and $M_{J2} \cdot \sigma$ (open circles), for $M_{10} \cdot \sigma$, $M_{J2} \cdot \sigma$ and $M_1 \sigma \cdot \nabla$ (filled circles), and with for $J = 1, 2, 3$ matrix elements (stars). The horizontal lines indicate the central value and error bar for the experimental result $A_L^{stat} = 0.60 \pm 0.11$.

REFERENCES

- [1] M. L. Goldberger and S. B. Treiman, Phys. Rev. **111**, 354 (1958).
- [2] V. Bernard, N. Kaiser and Ulf-G. Meissner, Phys. Rev. D **50**, 6899 (1994).
- [3] Harold W. Fearing, Randy Lewis, Nader Mobed, and Stefan Scherer, Phys. Rev. D **56**, 1783 (1997).
- [4] T. Gorringer and H. W. Fearing, Rev. Mod. Phys. **76**, 31 (2004).
- [5] J. Delorme, M. Ericson, A. Figureau, and C. Thévenet, Ann. Phys. (NY) **102**, 273 (1976).
- [6] J. Delorme and M. Ericson, Phys. Rev. C **49**, R1763 (1994).
- [7] M. Rho, Ann. Rev. Nucl. and Part. Science **34**, 531 (1984).
- [8] A. Possoz, D. Favart, L. Grenacs, J. Lehmann, P. Macq, D. Meda, L. Palffy, J. Julien, and C. Samour, Phys. Lett. B **50**, 438 (1974).
- [9] A. Possoz, Ph. Deschepper, L. Grenacs, P. Lebrun, J. Lehmann, L. Palffy, A. de Moura Gonclaves, C. Samour and V. I. Telegdi, Phys. Lett. B **70**, 265 (1977).
- [10] L.Ph. Roesch, V. L. Telegdi, P. Truttmann, A. Zehnder, L. Grenacs, and L. Palffy, Phys. Rev. Lett. **46**, 1507 (1981).
- [11] Y. Kuno, J. Imazato, K. Nishiyama, K. Nagamine, T. Yamazaki, and T. Minamisono, Phys. Lett. B **148**, 270 (1984).
- [12] V. Brudanin *et al.*, Nucl. Phys. A **587**, 577 (1995).
- [13] B.A. Moftah, E. Gete, D. F. Measday, D. S. Armstrong, J. Bauer, T. P. Gorringer, B. L. Johnson, B. Siebels, and S. Stanislaus, Phys. Lett. B **395**, 157 (1997).
- [14] Ch. Briançon *et al.*, Nucl. Phys. A **671**, 647 (2000).
- [15] J.P. Deutsch, L. Grenacs, J. Lehmann, P. Lipnik, and P. C. Macq, Phys. Lett. B **28**, 178 (1968).
- [16] V. Wiaux, R. Prieels, J. Deutsch, J. Govaerts, V. Brudanin, V. Egorov, C. Petitjean, and P. Truöl, Phys. Rev. C **65**, 025503 (2002).
- [17] T.P. Gorringer, B.L. Johnson, D.S. Armstrong, J. Bauer, M.D. Hasinoff, M.A. Kovash, D.F. Measday, B.A. Moftah, R. Porter, and D.H. Wright Phys. Rev. Lett. **72**, 3472 (1994).
- [18] B.L. Johnson, T. P. Gorringer, D. S. Armstrong, J. Bauer, M. D. Hasinoff, M. A. Kovash, D. F. Measday, B. A. Moftah, R. Porter, and D. H. Wright, Phys. Rev. C **54**, 2714 (1996).
- [19] J.P. Deutsch, L. Grenacs, J. Lehmann, P. Lipnik, and P. C. Macq, Phys. Lett. B **29**, 66 (1969).
- [20] F.R. Kane, M. Eckhause, G. H. Miller, B. L. Roberts, M. E. Vislay, and R. E. Welsh, Phys. Lett. B **45**, 292 (1973).
- [21] P. Guichon, B. Bihoreau, M. Giffon, A. Gonçalves, J. Julien, L. Roussel, and C. Samour, Phys. Rev. C **19**, 987 (1979).
- [22] T.J. Stocki, D.F. Measday, E. Gete, M.A. Saliba, B.A. Moftah and T.P. Gorringer Nucl. Phys. A **697**, 55 (2002).
- [23] L. Grenacs, J.P. Deutsch, P. Lipnik, and P.C. Macq, Nucl. Instrum. Methods **58**, 164 (1968).
- [24] F. Ajenberg-Selove, Nucl. Phys. A **253**, 1 (1991).
- [25] SRIM program, J.F.Ziegler. See J.P. Biersack, J.F. Ziegler and U. Littmark, *The stopping and range of ions in solids*, Pergamon Press (1985).
- [26] A.P. Bukhvostov and N.P. Popov Phys. Lett. B **24**, 497 (1967).

- [27] A.P. Bukhvostov and N.P. Popov, Nucl. Phys. A **147**, 385 (1970).
- [28] T.A. Dmitrieva, Z. Oziewicz, A. Pikulski Nucl. Phys. A **155**, 205 (1970).
- [29] S. Ciechanowicz and Z. Oziewicz, Fortsch. Phys. **32**, 61 (1984).
- [30] G. Culligan, J. F. Lathrop, V. L. Telegdi, R. Winston, and R. A. Lundy, Phys. Rev. Lett. **7**, 458 (1961).
- [31] R. Winston, Phys. Rev. **129**, 2766 (1963).
- [32] K. Ishida, J. H. Brewer, T. Matsuzaki, Y. Kuno, J. Imazato and K. Nagamine, Phys. Lett. B **167**, 31 (1986).
- [33] Evaluated Nuclear Structure Data File (8/1/2004). National Nuclear Data Center, Brookhaven National Laboratory.
- [34] B. Krusche *et al.*, Nucl. Phys. A **386**, 245 (1982).
- [35] S. Aroua *et al.*, Nucl. Phys. A **720**, 71 (2003).
- [36] E.K. Warburton and W.T. Pinkston, Phys. Rev. **118**, 733 (1960).
- [37] H.-G. Clerc and E. Kuphal, Zeitschrift fur Physik **211**, 452 (1968).
- [38] S. Lie, Nucl. Phys. A **181**, 517 (1972).
- [39] A.I. Babaev *et al.*, JINR Report R-14-42-41 (1968), quoted in V.A. Vartanyan *et al.*, Sov. J. Nucl. Phys. **11**, 295 (1970).
- [40] M.N. Thompson, R.J.J. Stewart and J.E.M. Thompson Phys. Lett. B **31**, 211 (1970).
- [41] E. Belotti *et al.*, SIN Newsletter **1**, 4, (1976), quoted in N.C. Mukhopadhyay, Phys. Rep. **30C**, 1 (1977).
- [42] M. Giffon, A. Goncalves, P. A. M. Guichon, J. Julien, L. Roussel and C. Samour, Phys. Rev. C **24**, 241 (1981).
- [43] A.P. Bukhvostov, A.M. Chatrchyan, G.E. Dogotar, R.A. Eramzhyan, N.P Popov and V.A. Vartanjan Acta Phys. Pol. B **3**, 375 (1972).
- [44] N.C. Mukhopadhyay, Phys. Lett. B **44**, 33 (1973).
- [45] N.C. Mukhopadhyay, Phys. Lett. B **45**, 309 (1973).
- [46] H.R. Kissener, A. Aswad, H.U. Jager and R.A. Eramzhian Nucl. Phys. A **215**, 424 (1973).
- [47] P. Desgrolard, P. A. M. Guichon and J. Joseph, Nuovo Cim. A **43**, 475 (1978).
- [48] P. Desgrolard and P. A. M. Guichon, Phys. Rev. C **19**, 120 (1979).
- [49] N. Auerbach and B. A. Brown, Phys. Rev. C **65**, 024322 (2002).
- [50] S. Cohen and D. Kurath, Nucl. Phys. **73**, 1 (1965).
- [51] W. Chung, Ph.D. thesis, Michigan State University, 1976 (unpublished).
- [52] D.J. Millener and D. Kurath, Nucl. Phys. A **255**, 315 (1975).
- [53] E. K. Warburton and D. J. Millener, Phys. Rev. C **39**, 1120 (1989).
- [54] M. Morita and A. Fujii, Rev. Phys. **118**, 606 (1960).
- [55] J.D. Walecka, in Muon Physics, C.S. Wu and V. Hughes eds., Academic Press, NY, (1975).
- [56] B.A. Brown, A. Etchegoyen, W. D. M. Rae, and N. S. Godwin, MSUCL Report No. 524 (1986).
- [57] T.W. Donnelly and W.C. Haxton, At. Data Nucl. Data Tables **23**, 103 (1979).
- [58] M. Morita, and A. Fujii, Phys. Rev. **118**, 606 (1960).